JACS
JOURNAL OF THE AMERICAN CHEMICAL SOCIETY
Article
pubs.acs.org/JACS

Probing the Interaction of Single Nanocrystals with Inorganic Capping Ligands: Time-Resolved Fluorescence from CdSe–CdS Quantum Dots Capped with Chalcogenidometalates

Amy A. Cordones,[†,§,#,∥] Marcus Scheele,[†,§,∥] A. Paul Alivisatos,*[,†,§] and Stephen R. Leone*[,†,‡,§,#]

[†]Department of Chemistry, and [‡]Department of Physics, University of California, Berkeley, California 94720, United States
[§]Material Sciences Division and [#]Chemical Sciences Division, Lawrence Berkeley National Laboratory, Berkeley, California 94720, United States

Supporting Information

ABSTRACT: Fluorescence intermittency and excited-state decay measurements are carried out on single CdSe–CdS core–shell quantum dots (QD) stabilized with chalcogenidometalates (ChaMs, $In_2Se_4^{2-}$, or $Sn_2S_6^{4-}$)$^-$. The results are used to probe the nature and distribution of charge trapping sites in the QD local environment. A comparison is made between capping by a neutral organic ligand (oleylamine) and a small inorganic ligand with high charge density (ChaMs). Overall, shorter on-state durations and longer off-state durations are observed for the ChaMs. These results indicate an increased density of charge trapping sites and increased stabilization of surface-trapped charges. By varying the thickness of the CdS shell, we identified hole trapping by the ligand as the dominant charging mechanism in ChaM-capped QDs. Faster excited-state decay rates are measured for the ChaM-capped QDs, highlighting the role of strongly stabilized trapped charges in this system. Using cyclic voltammetry measurements of the ChaMs, an energy level diagram is constructed relating the ChaMs and CdSe–CdS-QDs that explains their superior performance as active layers in photodetectors.

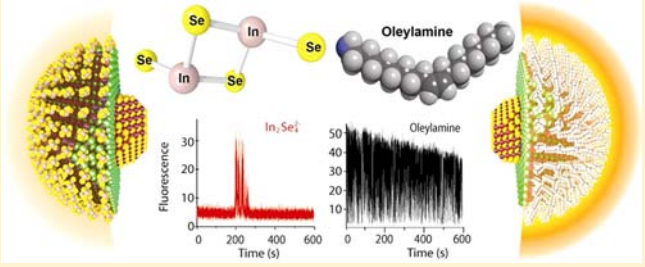

1. INTRODUCTION

Chalcogenidometalates (ChaMs) are known for their rich coordination chemistry, semiconducting behavior, and strong binding affinity to heavy metal ions.[1,2] These properties are manifested in their successful application as capping ligands for metal and semiconductor nanocrystals.[3] Excellent colloidal stability in solvents of either high basicity or dielectric constant like hydrazine, aqueous ammonia, or formamide occurs, allowing for solution-processed and low-cost pathways to uniform nanoparticle thin films and self-assembled superlattices.[4,5] In some cases, extraordinary high field-effect mobilities are observed for such films, attributed to favorable energy alignment between the constituent nanoparticles and ligands. For example, electron mobilities greater than 30 $cm^2/V{\cdot}s$ were recently reported for $In_2Se_4^{2-}$-capped CdSe nanocrystals.[6] This opens exciting possibilities for applications of nanoparticle thin films in (opto-) electronic devices of which field-effect transistors (FETs) with on/off ratios $>10^3$ and photodetectors with detectivities $D^* > 10^{13}$ $cm{\cdot}Hz^{1/2}/W$ were demonstrated so far.[7] The optical properties of such films were studied as well.[8]

In contrast to the aforementioned ongoing studies of collective properties of ChaM-capped semiconductor nanocrystals, very little is known about isolated ChaM–nanocrystal systems. A recent theoretical study on $Sn_2S_6^{4-}$-linked CdSe nanoparticle dimers is the main contribution to this topic so far.[9]

Time-resolved fluorescence intermittency and excited-state decay microscopy of single nanoparticles is a powerful tool to study some of the fundamental processes governing the photophysics on a single nanoparticle level, such as exciton generation and decay, nanoparticle–ligand coupling, and the nature and density of trap states.[10] In particular, fluorescence intermittency (hereafter referred to as "blinking") is a universal property of molecular emitters such as nanocrystal quantum dots (QDs).[11] Although the exact mechanism responsible for QD blinking is not known, charge localization at trapping sites within or external to the QD is widely accepted as a cause of the QD switching from the fluorescent "on-"state to the dim "off-"state. In this regard, statistical analysis of the on-state blinking behavior is frequently applied to yield information regarding the nature of and accessibility to electron and hole trapping sites upon variation of the shell material or surface capping ligand of the QD.[12,13] Furthermore, the interaction of the surface trapped charge with various dielectric environments can be successfully probed by analysis of the off-state blinking behavior.[14,15] On the basis of this, the blinking statistics of QD emitters are expected to undergo significant changes when a

Received: July 22, 2012
Published: October 17, 2012

   dx.doi.org/10.1021/ja3071732 | J. Am. Chem. Soc. 2012, 134, 18366–18373

nonpolar, insulating, and long-chained organic ligand is exchanged for a ChaM that has a relatively high charge density and narrow spacing between the highest occupied and lowest unoccupied molecular orbitals (HOMO/LUMO).

In the present work, individual CdSe–CdS nanoparticles capped with tetraselenidoindate ($In_2Se_4^{2-}$) or hexasulfidostannate ($Sn_2S_6^{4-}$) are investigated. The structural, optical, and electrochemical characterizations of the QD–ligand systems are discussed, and electronic energy level diagrams are constructed for the two types of ChaM-capped QDs. Time-resolved fluorescence spectroscopy of individual ChaM-capped QDs is applied to investigate the change in the nature and distribution of charge trapping sites on the QD surface upon ligand exchange from oleylamine (OA) to the ChaM complexes. Increased hole trapping rates and a high stability of trapped holes are observed for the ChaM-stabilized QDs, resulting in a dramatic decrease in the percentage of time spent in the on-state relative to QDs with OA capping. The high stability of ligand-trapped holes is emphasized through the observation of very long off-state durations and enhanced fluorescence decay rates of ChaM-capped QDs. This information is of fundamental interest for applying such functionalized QDs as the active material in optoelectronic devices such as photodetectors.

2. EXPERIMENTAL SECTION

For experimental details on QD synthesis, description of characterization techniques, and sample preparation, the reader is referred to the Suporting Information. A thorough description of the confocal fluorescence microscope was previously reported,[16,17] and further details are in the Supporting Information. Briefly, the blinking studies are conducted in a wide-field illumination mode with a 405 nm continuous excitation source and a charge coupled device (CCD) camera for signal detection with 33.4 ms time resolution. The fluorescence decay curves reported in section 3.3 are measured simultaneously with blinking through the use of a time-tagged time-resolved single photon counting card. Those experiments employ a 500 nm pulsed excitation source and single photon counting avalanche photodiode (APD) detectors, yielding ~40 ps time resolution (instrument response limited).

For the blinking data analysis, a threshold is set to distinguish the on- and off-states for each single QD blinking trace.[16] The blinking trace is then broken into a series of on- and off-state durations. A weighted probability distribution of off- or on-state durations is constructed, where the probability is divided by the average time to the next longest and next shortest durations.[18] The off-state probability distributions are well described using an inverse power law, with a power law coefficient α_{off}.

The on-state probability distributions are observed to decay by a power law for short durations and exponentially for long durations. The log–log data are binned by duration and averaged to produce an equally weighted data set across the full range of on-state durations, which typically span several orders of magnitude. The binned data are fit using eq 1 to obtain the power law coefficient, α_{on}, and crossover time, τ_c.

$$P(t_{on}) \propto t_{on}^{-\alpha_{on}} \exp(-t_{on}/\tau_c) \quad (1)$$

In this work, single ChaM-stabilized QDs are observed to have very few off-to-on switching events, resulting in sparsely populated probability distributions that cannot be reliably fit. To address this issue, probability distributions are generated from the combination of all on- and off-state durations of all QDs measured. This method provides one on- and one off-state probability distribution representing the combined behavior of many individually measured QDs. The results of this method are consistent with the average fits acquired from individual QD distributions.

3. RESULTS

3.1. Characterization and Energy Level Diagrams. The core shell CdSe–CdS QDs studied in this work closely resemble the QDs used in recent reports on the transport properties of ChaM-capped nanocrystals,[6,7] apart from a smaller core diameter (2.5 nm vs 4 nm) used in the present work. We chose $In_2Se_4^{2-}$ and $Sn_2S_6^{4-}$ for the ligand exchange starting from OA capping because these are the most widely applied ChaMs in this respect. To study the effect of CdS shell thickness on the coupling between the CdSe core and ChaM ligand, two sets of nanoparticle samples are prepared following the established procedure by Mahler et al.;[23] TEM micrographs and size histograms are displayed in Figure 1. According to

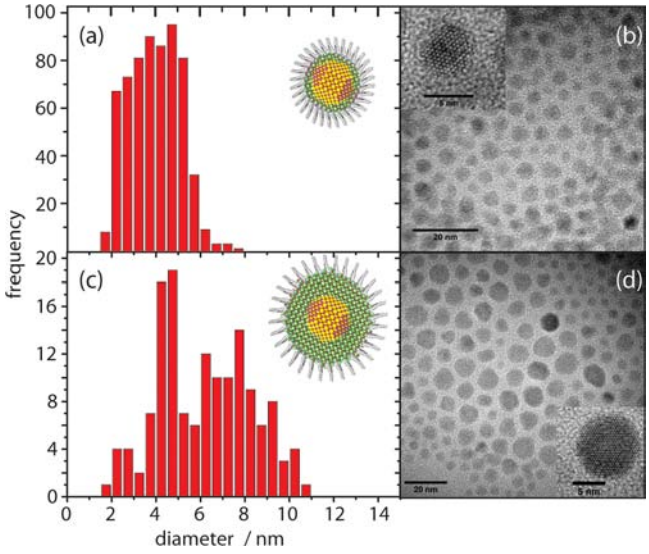

Figure 1. TEM micrographs and size histograms of the two QD samples (capped with OA) applied in this work. (a,b) 2.5 nm CdSe core and 3 monolayers of CdS shell. (c,d) 2.5 nm CdSe core and 8 monolayers of CdS shell. The shell thickness was inferred from the main particle diameter as displayed in the histograms in (a) and (c) and on using one-half the length of the hexagonal unit cell axis (~0.34 nm) per monolayer thickness in accordance with previous work.[19]

Chen et al., these core–shell particle sizes correspond to a nominal shell thickness of 3 monolayers (ML) for sample 1 and 8 ML for sample 2.[19] (From here on, we use the terms CdSe–3CdS for sample 1 and CdSe–8CdS for sample 2, respectively).

Upon ligand exchange of OA ligands with either $In_2Se_4^{2-}$ or $Sn_2S_6^{4-}$, excellent colloidal stability is observed over weeks in anhydrous hydrazine. TEM analysis shows the mean particle size and dispersion are unchanged in all cases except for samples annealed at temperatures greater 230 °C where a small degree of sintering is observed. Using X-ray diffraction (XRD) of annealed powder samples, we confirm the absence of crystalline domains of SnS_2 or In_xSe_y, indicative of carefully cleaned ChaM-capped QD samples without significant amounts of excess ligand present. We perform FT-IR analysis of all samples to verify the success of ligand exchange by the disappearance of the C–H bands.[24] For images supporting the characterization described above, the reader is referred to Figures S1–S8 in the Supporting Information.

In Figures 2a and b, we display cyclic voltammetric (CV) data on thin films of $(N_2H_5)_4Sn_2S_6$ and $(N_2H_5)_2In_2Se_4$ to estimate the position of the HOMO and LUMO levels. All values are stated with respect to the absolute vacuum level and

dx.doi.org/10.1021/ja3071732 | J. Am. Chem. Soc. 2012, 134, 18366–18373

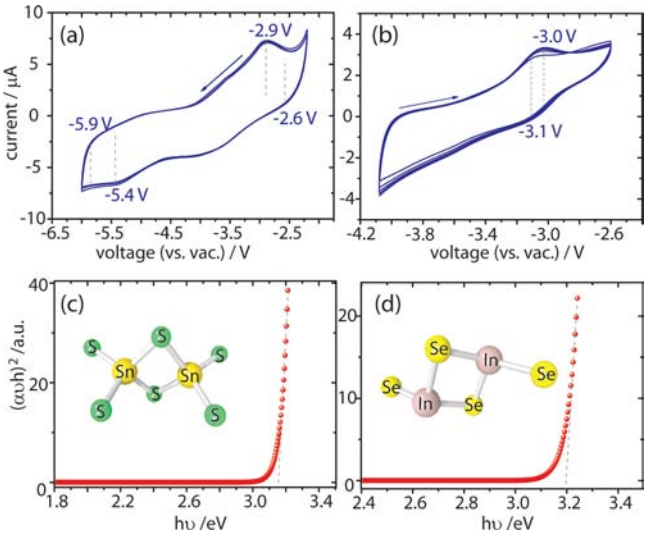

Figure 2. Cyclic voltammetry of (a) $(N_2H_5)_4Sn_2S_6$ and (b) $(N_2H_5)_2In_2Se_4$. All values of redox waves are stated with respect to the absolute vacuum level. Both plots are overlays of 10 consecutive scans at 50 mV/s. Note that in (b), only the cathodic side seen from the open circuit potential is displayed. Parts (c) and (d) show Tauc-plots according to ref 20 of $Sn_2S_6^{4-}$ and $In_2Se_4^{2-}$, respectively, with the absorbance α, Planck's constant h, and the frequency of the incident photons ν. The ball-and-stick-models represent the molecular structure of the two ChaMs as previously reported.[21,22]

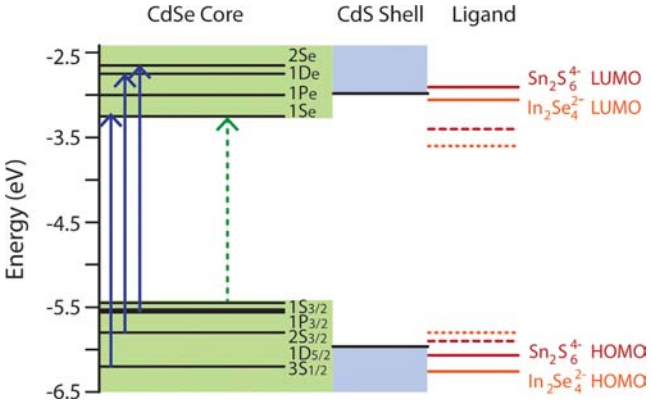

Figure 3. Energy level diagram for ChaM-capped CdSe−CdS QDs obtained as specified in the text. Scale relative to the absolute vacuum level. For the ChaMs, solid lines represent $N_2H_5^+$-complexes, whereas dotted and dashed lines stand for the Cd^{2+}-analogues of the $In_2Se_4^{2-}$-anion and $Sn_2S_6^{4-}$-anion, respectively. Arrows indicate highest allowed excitation transitions during blinking (solid blue arrows, λ_{ex} = 405 nm) and fluorescence decay (dashed green arrow, λ_{ex} = 500 nm) experiments according to previous measurement.[28]

are derived by using ferrocene as an internal reference. For $(N_2H_5)_4Sn_2S_6$, we obtain a LUMO position of −2.8 eV and the HOMO at −5.7 eV, and thus an electrochemical energy gap of 2.9 eV. For $(N_2H_5)_2In_2Se_4$, we find a fully reversible oxidation/reduction feature in the cathodic direction with a midpoint potential of −3.1 V that is attributed to the LUMO position. In contrast, no stable feature in the anodic direction could be captured.

To determine the optical energy gap for the ChaMs applied in this work, we use the Tauc relationship for direct allowed transitions and estimate the gap from the *x*-axis intercept in the plots in Figures 2c and d.[20] We obtain E_{Gap} = 3.15 eV for $Sn_2S_6^{4-}$ and E_{Gap} = 3.20 eV for $In_2Se_4^{2-}$ in anhydrous hydrazine.

Binding to the surface of CdSe−CdS QDs could potentially change the energy level positions of the ChaMs. To address this effect, we also measure the energy levels of $Cd_2Sn_2S_6$ and $CdIn_2Se_4$ with CV (Figure S9). We find the HOMO/LUMO at −5.9 eV/−3.4 eV for $Cd_2Sn_2S_6$ and at −5.8 eV/−3.6 eV for $CdIn_2Se_4$. The two pairs of ChaM-species characterized by CV throughout this Article should be viewed as extreme boundaries to the realistic scenario of free ChaMs bound to QD surface cadmium. It is likely that the degree of electron donation by the ChaM is underestimated for the N_2H_5−ChaMs, but overestimated for the Cd−ChaMs.

On the basis of the optical and electrochemical data in this work and the energy level positions in CdSe QDs found in the literature, we arrive at the energy level diagram displayed in Figure 3. We refer to Jasieniak et al. and the absorbance data reported here for the absolute energy of the $1S_{3/2}$ and $1S_e$ levels of CdSe, respectively,[25] Efros and Rosen for the intraband spacing of the S-, P-, and D-levels,[26] and Peng et al. for the offsets between the CdSe and CdS conduction and valence band edges.[27] The LUMO positions of ChaMs are inferred from our CV data, whereas the HOMO positions are calculated by adding the optical energy gap. We also display the HOMO/LUMO positions of the corresponding Cd−ChaMs derived from CV for comparison.

From the energy level diagram, it is postulated that the ChaM complexes may be capable of receiving both electrons and holes from the photoexcited QD at the excitation energy of the 405 nm laser used here. The fluorescence blinking statistics of single QDs are used to quantify the change in distribution of charge trapping sites upon QD stabilization by the ChaMs. Variation of the CdS shell thickness is employed as a means to distinguish between the electron or hole trapping nature of these sites.

3.2. Fluorescence Blinking of ChaM-QDs. There are several changes in the fluorescence blinking behavior upon exchange of the QD ligand from OA to either of the two ChaM complexes used here. Overall, dramatically less fluorescence is observed from the ChaM-stabilized QD samples. This is the result of both an increase in the percentage of time spent in the off-state, as well as a decreased quantum yield (QY) of the fluorescent on-state. Figure 4a compares 10 min of blinking behavior for an OA-QD and an $In_2Se_4^{2-}$-QD, typical of a larger sampling of each type of QD. While the OA-QDs are observed to spend the majority of time in the highly fluorescent on-state, the $In_2Se_4^{2-}$-QDs are found to rarely fluoresce, spending the majority of the time in the off-state. The decreased fluorescence observed here for both ChaM-QD samples is consistent with reports of decreased QY in large ensembles of similar QDs upon ligand exchange from organic to ChaM stabilization.[4,8] We next consider the ligand-dependent changes in the blinking behavior (OA versus both ChaM ligands) for the two QD samples of different CdS shell thicknesses. On the basis of the results presented below, we suggest that the ChaMs studied in this work act as long-lived traps for holes generated inside the QD, which critically dominates the optoelectronic properties of ChaM-capped QDs. Excited-state decay times are also compared for the two classes of ligands, the results of which highlight the stability of surface trapped holes in the ChaM-QD samples.

Blinking Analysis of CdSe−8CdS QDs. The blinking statistics are compared in Figure 4 for CdSe−8CdS stabilized

dx.doi.org/10.1021/ja3071732 | J. Am. Chem. Soc. 2012, 134, 18366−18373

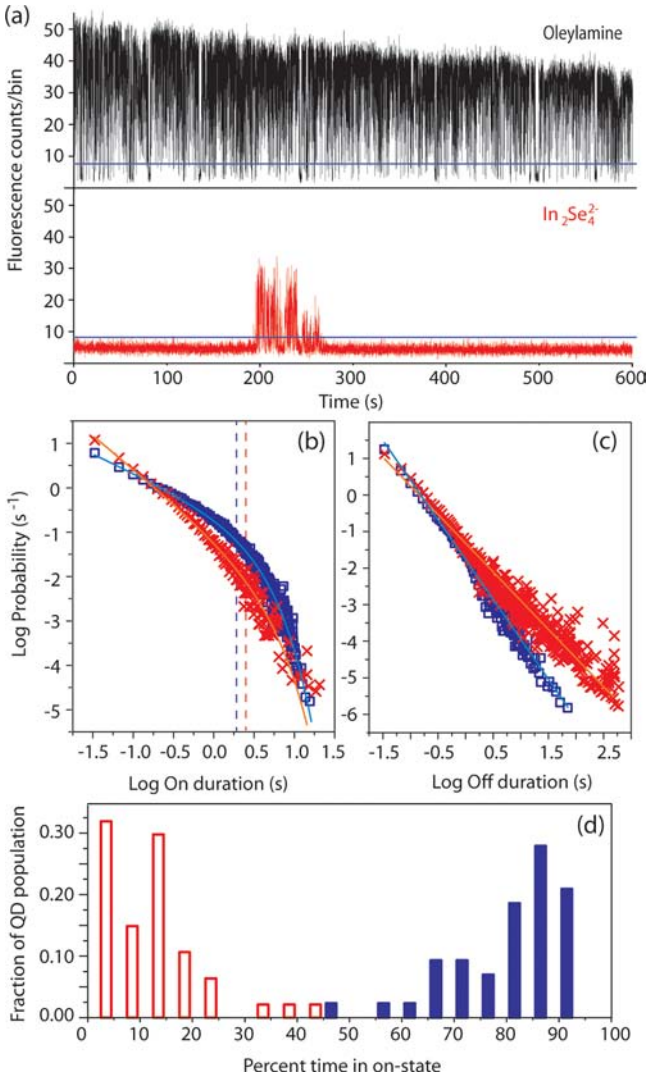

Figure 4. Fluorescence blinking analysis of CdSe−8CdS QDs capped with OA and $In_2Se_4^{2-}$ (λ_{ex} = 405 nm, 575 W/cm^2). (a) 10 min blinking traces for a single OA-QD (black) and $In_2Se_4^{2-}$-QD (red). Solid blue lines indicate the on/off state threshold. (b)−(d) Blinking statistics of 43 OA-QDs (blue squares) and 47 $In_2Se_4^{2-}$-QDs (red Xs). (b) On-state duration probability distributions. Solid lines indicate fits to eq 1. τ_c values are indicated by dashed lines (note that the four longest on-state durations for the $In_2Se_4^{2-}$-QD distribution were ignored to yield a better fit to the midlength durations, which are more relevant in determining τ_c). (c) Off-state duration probability distributions. Solid lines indicate fits to an inverse power law. (d) Percent time spent in the on-state for OA-QDs (blue solid bars) and $In_2Se_4^{2-}$-QDs (red open bars).

by OA and $In_2Se_4^{2-}$. Overall, similar on-state duration probability distributions are observed for the two ligands. However, much longer off-state durations are observed for the $In_2Se_4^{2-}$-QDs.

The on-state probability distributions are interpreted in terms of the charge trapping rate of the sample, where a smaller crossover time value (τ_c) indicates faster charge trapping and, therefore, greater accessibility to trapping sites. A slightly faster decay of the short on duration probability distribution (larger α_{on}) is observed for the $In_2Se_4^{2-}$-QDs, but, more notably, very similar τ_c values (1.92 ± 0.03 s for OA and 2.5 ± 0.3 s for $In_2Se_4^{2-}$, see dashed lines in Figure 4b) and maximum on-state durations (15.6 s for OA and 20.5 s for $In_2Se_4^{2-}$) are observed for the two samples. The similar on-state statistics suggests that the accessibility to the charge trapping sites on the QD surface is dominated by the energy level offsets for the CdSe core and CdS shell materials, which are inherently identical for both systems. It is expected that the hole is highly confined to the CdSe core, while the electron may extend into the CdS shell. Therefore, these initial results hint that changes in the blinking behavior upon exchanging the OA ligand for the $In_2Se_4^{2-}$ complex may lead to an increase in hole trapping sites, but there is little or no change in the distribution of electron trapping sites.

As a result of the longer off-state durations, the power law coefficient decreases from α_{off} = 2.17 ± 0.03 for the OA-QDs to α_{off} = 1.57 ± 0.03 for $In_2Se_4^{2-}$-QDs (Figure 4c). This trend suggests an increased stability of the surface trapped charges by the $In_2Se_4^{2-}$ ligand. The stabilization results in the very small percentage of time spent in the on state, as shown in Figure 4d. On average, the OA-QDs spend 81.5 ± 1.6% of the time in the on state, while the $In_2Se_4^{2-}$-QDs spend only 11.1 ± 1.4% time in the on state (errors are one standard deviation of the mean).

Blinking Analysis of CdSe−3CdS QDs. We test the preliminary hypothesis of hole trapping in the ChaM ligands by reducing the CdS shell thickness. Blinking statistics are measured for CdSe−3CdS, stabilized by both ChaM complexes and OA. The thinner CdS shell allows for increased accessibility of the hole to the surface ligands, as compared to the CdSe−8CdS QDs. Overall, a dramatic shift to shorter on-state durations is observed for the $In_2Se_4^{2-}$ capped CdSe−3CdS QDs. Longer off-state durations are also observed for $In_2Se_4^{2-}$ stabilization, similar to the thicker shell samples.

The on-state probability distributions for OA-QDs and $In_2Se_4^{2-}$-QDs are shown for the 3 ML samples in Figure 5a.

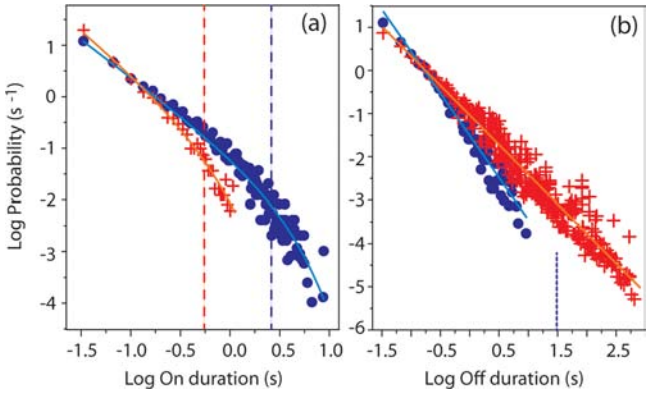

Figure 5. Blinking statistics of 34 OA-capped (blue ●) and 31 $In_2Se_4^{2-}$-capped (red +) CdSe−3CdS QDs. (a) On-state duration probability distributions. τ_c values are indicated by dashed lines. (b) Off-state duration probability distributions. Because of photobleaching, the OA-QD data are calculated from the first 30 s of the blinking traces (dashed line indicates the 30 s limit). For detailed analysis of photobleaching in both samples, the reader is referred to Figure S10 and the Supporting Information.

Ligand exchange from OA to $In_2Se_4^{2-}$ causes a dramatic increase in the charge trapping rate, as indicated by decreases in both τ_c, from 2.0 ± 0.1 to 0.54 ± 0.09 s, and in the longest observed on-state durations, from 8.8 to 1.1 s. The increase in trapping rate observed here, but not for the thick CdS shell, indicates the hole is the most likely carrier trapped by the ChaM ligand.

dx.doi.org/10.1021/ja3071732 | J. Am. Chem. Soc. 2012, 134, 18366−18373

The off-state probability distributions are shown for both CdSe−3CdS samples in Figure 5b. (Only the first 30 s of blinking data is used in the off-state analysis for the OA-capped CdSe−3CdS QDs to account for the photobleaching observed in this sample; for details, the reader is referred to Figure S10 in the Supporting Information.) Ligand exchange to $In_2Se_4^{2-}$ leads to longer off-state durations with $\alpha_{off} = 1.95 \pm 0.06$ for OA and $\alpha_{off} = 1.37 \pm 0.02$ for $In_2Se_4^{2-}$ stabilization.

No significant differences are observed in the blinking behavior of the CdSe−3CdS QDs stabilized with the two ChaM ligands. Additionally, no difference is observed for the $Sn_2S_6^{4-}$-capped CdSe−3CdS QDs annealed at temperatures above and below the decomposition point of this stannate compound (roughly 200 °C).[21] This lack of variation indicates there is no change in the local environment of the QD and that there is no observed decomposition of $Sn_2S_6^{4-}$ to SnS_2 on these isolated QD samples without excess ligand. For detailed comparisons of the above samples, the reader is referred to the Supporting Information and Figures S11 and S12.

CdS Shell Thickness Dependence. A comparison of the CdS shell thickness dependence of the blinking statistics for each surface ligand is shown in Figure 6a-c. The on- and off-state

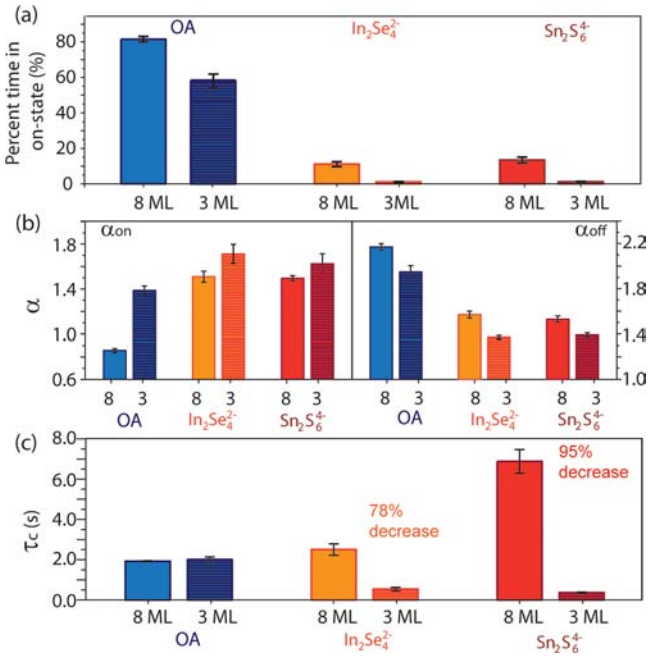

Figure 6. Blinking statistics for two CdS shell thicknesses and all three stabilizing ligands. In all panels, the CdSe−8CdS QDs are indicated by solid bars and the CdSe−3CdS QDs are indicated by striped bars. OA-QDs are shown in blue, $In_2Se_4^{2-}$-QDs are orange, and $Sn_2S_6^{4-}$-QDs are red. (a) Average percent time spent in the on state. Full range of error bars are two standard deviations of the mean. (b) On- and off-state power law coefficients (α). (c) Crossover time (τ_c) of the on-state distribution. (b,c) Error bars are plus and minus one standard deviation of the fit parameters.

duration probability distributions are shown in Figure S13, and fit parameters are listed in Table S1 of the Supporting Information for each shell thickness and ligand. Generally, the results reported here are consistent with several studies comparing blinking statistics of QDs with varying shell thickness, stabilized by organic ligands.[23,29−31] Specifically, the thicker CdS shell QDs spend more time in the on state for all three ligands (see Figure 6a).[23,29,31] Also consistent with previous work, Figure 6b illustrates a decrease of α_{on} and increase of α_{off} with increasing shell thickness.[29,30]

The trend in τ_c values for the on-state distributions of the thin and thick CdS shells reveals an interesting difference between the OA- and ChaM-stabilized QDs (see Figure 6c). Decreasing the CdS shell does not lead to any significant change in the τ_c value for the OA-QD samples, which suggests that the increased surface access of the hole does not lead to enhanced trapping. Therefore, it is likely that charge trapping at the core/shell interface or surface electron trapping accounts for the blinking in these samples. In contrast, the ChaM results show that decreasing the CdS shell thickness leads to a 78% decrease in τ_c for the $In_2Se_4^{2-}$-QDs and a 95% decrease in τ_c for the $Sn_2S_6^{4-}$-QDs. For both ChaM-stabilized QDs, increased surface access of the hole leads to greatly enhanced trapping rates. This trend is consistent with an increase in available hole trapping sites upon QD stabilization using the ChaM complexes. The nature of the different charge trapping sites for the two ligands is considered further in section 4, as are the implications of this result for the application of ChaM-capped QDs.

3.3. Excited-State Decay of ChaM-QDs. Excited-state decay curves are recorded simultaneously with the blinking traces for single CdSe−8CdS QDs stabilized by both OA and $In_2Se_4^{2-}$. Decay curves are constructed separately for photons arriving during the on and off states. Although the off state is often considered to be nonfluorescent, a low level of fluorescence is emitted.[17,32,33]

Figures 7a and b show the excited-state decays for the on and off states of the OA- and $In_2Se_4^{2-}$-capped QDs. This plot

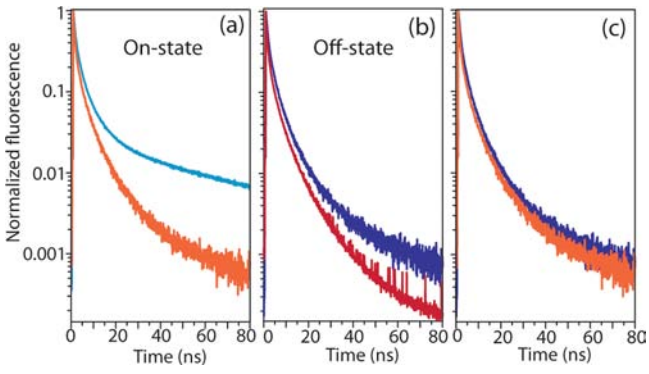

Figure 7. Averaged fluorescence decay curves for $In_2Se_4^{2-}$ and OA-capped CdSe−8CdS QDs (λ_{ex} = 500 nm). Note the same scale on both axes for (a)−(c). (a) On-state decays for OA-QDs (cyan) and $In_2Se_4^{2-}$-QDs (orange). (b) Off-state decays for OA-QDs (blue) and $In_2Se_4^{2-}$-QDs (red). (c) On-state decay for $In_2Se_4^{2-}$-QDs (orange) overlaid with off-state decay for OA-QDs (blue).

represents the average behavior of 12 OA-QDs and 14 $In_2Se_4^{2-}$-QDs measured at a high excitation power density corresponding to a high per pulse probability of generating multiple excitons, $P(n \geq 2)$, approaching unity. A high occurrence of biexciton radiative recombination is observed (for detailed confirmation, the reader is referred to the Supporting Information and Figure S14). The decays measured here are all found to be multiexponential, likely due to the contributions of the single, bi-, and charged exciton (trion) emission.[34] The data could be adequately fit to three exponentials, and the decay times with fit errors and pre-exponential factors are listed in Table 1. We attribute the faster

dx.doi.org/10.1021/ja3071732 | J. Am. Chem. Soc. 2012, 134, 18366−18373

Table 1. Fit Parameters for Average On- and Off-State Decays of $In_2Se_4^{2-}$ and OA-Capped CdSe−8CdS QDs

	OA		$In_2Se_4^{2-}$	
	on-state	off-state	on-state	off-state
N_1	0.60	0.53	0.41	0.30
τ_1 (ns)	0.845 (±0.002)	0.710 (±0.003)	0.301 (±0.003)	0.19 (±0.02)
N_2	0.37	0.41	0.43	0.51
τ_2 (ns)	4.03 (±0.01)	2.93 (±0.02)	1.5 (±0.01)	1.00 (±0.01)
N_3	0.032	0.067	0.16	0.19
τ_3 (ns)	45.7 (±0.3)	10.7 (±0.1)	6.53 (±0.04)	5.16 (±0.02)
τ_{eff} (ns)	3.4 (±0.4)	2.28 (±0.04)	1.76 (±0.01)	1.55 (±0.01)

decay components to nonradiative Auger decay of the biexciton and possibly charged exciton species, and the slowest decay component to radiative recombination of the neutral biexciton, to be consistent with the literature.[34]

Comparing the on-state decay curves for the two ligands (see Figure 7a), we observe a faster decay rate for the $In_2Se_4^{2-}$-QDs, as compared to the OA-QDs. The fitted data in Table 1 indicate decreases in all three decay components with the ChaM ligand, as well as a decrease in the relative contribution of the slowest component. Taken together with the decreased fluorescence quantum yield observed for $In_2Se_4^{2-}$-capped QDs, these results suggest an increase in nonradiative decay pathways for the $In_2Se_4^{2-}$-QDs. Faster decay is also observed during the off state for the $In_2Se_4^{2-}$-QDs, as compared to the OA-QDs (see Figure 7b), indicated again by decreases in all three decay times and in the relative contribution of the slowest decay component. Possible mechanisms for increased decay rates are considered in section 4 and are related to the blinking behavior observed for the two ligands.

4. DISCUSSION

On the basis of the results presented above, we suggest that the ChaMs studied in this work act as long-lived traps for holes generated inside the QD, which critically dominates the optoelectronic properties of ChaM-capped QDs. The nature of the ligand-induced trapping sites is discussed here, followed by the implications of these results for the use of ChaMs-capped QDs in optoelectronic devices.

Nature of Trapping Sites for ChaM-Capped QDs. The different nature of the trapping sites for the QDs stabilized by the OA ligand or ChaM complexes is now considered, starting with the OA-QDs. Previous FT-IR studies of amine-capped CdSe QDs indicate that the amine groups bind to both the surface Se and Cd sites in a ratio of 60:40, suggesting that slightly more electron-trapping Cd cations are available on the QD surface.[8] Furthermore, optically detected magnetic resonance (ODMR) studies of CdSe/CdS QDs stabilized with dodecylamine report the observation of electron trapping sites located at the core/shell interface of the QD.[35] The lack of significant change in the charge trapping rate observed here in the OA-QDs as the CdS shell is varied (Figure 6c) is consistent with electron trapping at the core/shell interface or in the surface Cd sites.

In considering charge trapping sites for ChaM-stabilized QDs, previous reports of fluorescence measured for thiolate-stabilized QDs are relevant. An analogy can be drawn between the S^- group of the thiolate, which is thought to form a covalent bond with a surface Cd cation, and the Se^- and S^- groups of the $In_2Se_4^{2-}$ and $Sn_2S_6^{4-}$ complexes. Fluorescence blinking studies of CdSe QDs with several shell compositions, stabilized by a variety of water-soluble thiolate ligands, report a decrease in α_{off} and an increase in α_{on} for the thiolate-QDs as compared to organically stabilized QDs.[12,36] This is consistent with the present findings upon ligand exchange from OA to both ChaM complexes (see Figure 6b). Although the on-state probability distributions have been fit to an inverse power law,[12] it appears that truncation of the longer on-state durations occurs much earlier for the thiolate-QDs, similarly to what is observed in this work for the ChaM-stabilized CdSe−3CdS QDs. The authors interpret the changes in the blinking statistics to indicate an increase in the number of charge trapping sites, which they attribute to the two nonbonding electron pairs of the thiolate sulfur atom that act as hole traps. The similarity of the results presented here upon exchange from OA to ChaM ligands suggests that the Se^- and S^- groups of the ChaM complexes may bind to surface Cd cations, therefore increasing the number of hole trapping sites, which are attributed in this case to the nonbonding electron pairs on the selenium and sulfur atoms.

Highly Stabilized Trapped Holes. The high stability of the ligand-trapped hole in the ChaM-QDs is inferred from the very long off-state durations (and therefore small α_{off} values) observed in these samples, as compared to the OA-capped QDs. Highly stabilized trapped charges have previously been observed in CdSe/ZnS core/shell QDs dispersed in various polymers of high dielectric constants. Issac et al. report that an increased dielectric environment leads to longer off-state durations and smaller α_{off} values.[15] The authors assume a solvation model, where electrons trapped in intrinsic polymer states are highly stabilized by the more polarizable (high dielectric) environments. The data presented here (see Figure 6b) are consistent with that trend, based on the low dielectric constant of OA ($\varepsilon \approx 3.1$, measured at 2.45−5.8 GHz)[37] and the inference of a larger dielectric constant for the ChaM complexes from earlier work of Nag et al. showing that ChaMs are relatively soft ions with high polarizabilities.[38]

In contrast to the polymers discussed in ref 15, ChaMs possess a rich redox chemistry with the ability to form polychalcogenide chains of the nature Q_x^{2-} (where Q = S, Se, or Te).[1] We speculate that this ability facilitates the stabilization of photogenerated holes from the QDs in the ChaM ligand, possibly by oxidizing two chalcogenides to form a dichalcogenide bond according to $2RQ^- \rightarrow RQ{-}QR + 2e^-$. This redox process lies at the heart of chalcogenidometalate chemistry and has been shown to result in numerous structural variations from polyanionic chains, to rings and 3D-networks.[39] According to Figure 3, there is no significant driving force for permanent hole transfer from the QD into the ChaM ligand. This is reflected by our observation that ChaM-capped QDs do not photobleach within the experimental time frame and, therefore, are not being oxidized irreversibly. However, the redox process

dx.doi.org/10.1021/ja3071732 | J. Am. Chem. Soc. 2012, 134, 18366−18373

proposed here is largely reversible and could account for a long, but finite, stabilization of holes in the ChaM ligand.

The high stability of the ligand-trapped hole in $In_2Se_4^{2-}$-QDs is also reflected by the excited-state decay results presented in Figure 7 and Table 1. There are two plausible explanations for the observed change to faster decay times for the $In_2Se_4^{2-}$-QDs. First, we consider the stabilizing effect of the $In_2Se_4^{2-}$ ligand on surface trapped charges.

Under the high excitation intensities used for this measurement, an increase in the surface charging rate is expected due to biexciton Auger ionization.[16,40] Taken together with the longer lifetime of the trapped charges, one might expect a buildup of surface charges for the $In_2Se_4^{2-}$ capped QDs. It is therefore possible that the emission from both the high and the low intensity states for these samples is due to charged exciton decay.

In that case, the higher intensity state (on state) could be due to recombination of a singly charged exciton (one trapped charge), similar to the "gray state" of intermediate fluorescence intensity previously observed for nonblinking CdSe/CdS QDs,[41] while the lower intensity state would be due to recombination of a multiply charged exciton (more than one trapped charge). The shorter lifetime of the trapped charges in the OA-QDs may prevent the buildup of surface charges, such that the off state is due to a single trapped charge and the QD remains neutral during the on state. This explanation is supported by the similar decay times of the $In_2Se_4^{2-}$-QD on state and the OA-QD off state, which are plotted together in Figure 7c. We emphasize here again that this surface charge buildup holds true only under the high excitation intensity conditions used for the fluorescence decay measurements and not for the blinking experiments reported above. Future work measuring the excited-state decay rates as a function of excitation intensity could further elucidate the role of high order surface charging and Auger recombination for ChaM-stabilized QDs.

Alternatively, it is plausible that electron transfer from the CdSe conduction band to the LUMO of $In_2Se_4^{2-}$ could provide an additional nonradiative decay pathway, thus shortening the decay times for the $In_2Se_4^{2-}$-QDs, as compared to the OA-QDs. This possibility is considered less likely, however, as the measured $In_2Se_4^{2-}$ LUMO lies at slightly higher energy than is accessible by the 500 nm excitation.

ChaM-Capped QDs for Photodetectors. Using $In_2Se_4^{2-}$-capped CdSe–CdS nanocrystals, Lee et al. recently succeeded in fabricating one of the best nanocrystal-based photodetectors to date.[7] A good measure for the performance of a photodetector is its internal photoconductive gain (G_i). In an n-type material, G_i is proportional to the electron (majority carrier) mobility and the lifetime of the hole (minority carrier) before it recombines with an electron.[42] If the minority carrier is trapped sufficiently long, each photogenerated majority carrier can cycle several times through the device resulting in $G_i \gg 1$. This has been demonstrated for $In_2Se_4^{2-}$–CdSe–CdS with an impressive $G_i \geq 6.5 \times 10^3$. The two key factors responsible for this large value are explained by our results:

(1) The energy diagram derived in this work readily provides an explanation for the high electron mobilities due to resonance between the $1S_e$ level of CdSe and the LUMO of $In_2Se_4^{2-}$. Also, it has been demonstrated that $In_2Se_4^{2-}$-capped CdSe nanocrystals show significantly larger mobilities than comparable CdSe cores capped with $Sn_2S_6^{4-}$.[3,4,7] This is now supported by our CV data, which place the LUMO position of $Sn_2S_6^{4-}$ significantly higher in energy than that of $In_2Se_4^{2-}$.

(2) Lee et al. hypothetically attribute the long hole lifetimes in $In_2Se_4^{2-}$-capped CdSe–CdS QDs to the offset of the $1S_{3/2}$ levels between CdSe to CdS. The results presented here, however, argue that the dominant hole trapping site is not the core–shell interface but the ChaM ligand itself. In this work, the CdS shell thickness dependence of the charge trapping rate has identified the hole as the trapped carrier in the ChaM-QD samples. Furthermore, very long off-state durations were observed for the ChaM-capped QDs, indicating a high degree of stabilization of the surface-trapped hole by the ChaM ligands.

5. CONCLUSIONS

For the first time, the nature and distribution of charge trapping states in CdSe–CdS QDs capped with inorganic ChaMs are probed by single particle time-resolved fluorescence. In comparison to capping with a large and neutral organic ligand (oleylamine), dramatically shorter on-state durations are observed for the ChaM-stabilized CdSe–3CdS QDs, indicative of enhanced hole trapping rates. Furthermore, increased off-state probabilities are observed, which are attributed to efficient stabilization of the surface trapped holes. This hypothesis is further supported by the faster excited-state decay rates measured with ChaM stabilization, relative to OA. Using cyclic voltammetry, an energy level diagram for ChaM-capped QDs is constructed, which provides an immediate explanation for the successful application of this material in photodetectors.

■ ASSOCIATED CONTENT

Supporting Information

Detailed descriptions of experimental procedures, sample characterization supporting figures, and time-resolved fluorescence supporting figures. This material is available free of charge via the Internet at http://pubs.acs.org.

■ AUTHOR INFORMATION

Corresponding Author

*alivis@berkeley.edu; srl@berkeley.edu

Author Contributions

‖These authors contributed equally.

Notes

The authors declare no competing financial interest.

■ ACKNOWLEDGMENTS

We gratefully acknowledge financial support by the Physical Chemistry of Inorganic Nanostructures, KC3103, which is supported by the Director, Office of Science, Office of Basic Energy Sciences, U.S. Department of Energy under Contract No. DE-AC02-05CH11231 through the Materials Research Division. M.S. would like to thank the Alexander von Humboldt Foundation for a Feodor Lynen-Fellowship. Katie Lutker is gratefully acknowledged for providing the nanoparticles used in this work.

■ REFERENCES

(1) Sheldrick, W. S.; Wachhold, M. *Angew. Chem., Int. Ed. Engl.* **1997**, *36*, 206–224.

(2) Bag, S.; Trikalitis, P. N.; Chupas, P. J.; Armatas, G. S.; Kanatzidis, M. G. *Science* **2007**, *317*, 490–493.

(3) Kovalenko, M. V.; Scheele, M.; Talapin, D. V. *Science* **2009**, *324*, 1417−1420.
(4) Kovalenko, M. V.; Bodnarchuk, M. I.; Zaumseil, J.; Lee, J.-S.; Talapin, D. V. *J. Am. Chem. Soc.* **2010**, *132*, 10085−10092.
(5) Tangirala, R.; Baker, J.; Alivisatos, A.; Milliron, D. *Angew. Chem., Int. Ed.* **2010**, *49*, 2878−2882.
(6) Chung, D. S.; Lee, J.-S.; Huang, J.; Nag, A.; Ithurria, S.; Talapin, D. V. *Nano Lett.* **2012**, *12*, 1813−1820.
(7) Lee, J.-S.; Kovalenko, M. V.; Huang, J.; Chung, D. S.; Talapin, D. V. *Nat. Nanotechnol.* **2011**, *6*, 348−352.
(8) Zhang, Y. Q.; Cao, X. A. *Appl. Phys. Lett.* **2011**, *99*, 023106.
(9) Chu, I.-H.; Radulaski, M.; Vukmirovic, N.; Cheng, H.-P.; Wang, L.-W. *J. Phys. Chem. C* **2011**, *115*, 21409−21415.
(10) Jones, M.; Scholes, G. D. *J. Mater. Chem.* **2010**, *20*, 3533−3538.
(11) Nirmal, M.; Dabbousi, B. O.; Bawendi, M. G.; Macklin, J. J.; Trautman, J. K.; Harris, T. D.; Brus, L. E. *Nature* **1996**, *383*, 802−804.
(12) Kim, Y.; Song, N. W.; Yu, H.; Moon, D. W.; Lim, S. J.; Kim, W.; Yoon, H.-J.; Shin, S. K. *Phys. Chem. Chem. Phys.* **2009**, *11*, 3497−3502.
(13) Krogmeier, J. R.; Kang, H.; Clarke, M. L.; Yim, P.; Hwang, J. *Opt. Commun.* **2008**, *281*, 1781−1788.
(14) Bixby, T. J.; Cordones, A. A.; Leone, S. R. *Chem. Phys. Lett.* **2012**, *521*, 7−11.
(15) Issac, A.; von Borczyskowski, C.; Cichos, F. *Phys. Rev. B* **2005**, *71*, 161302.
(16) Cordones, A. A.; Bixby, T. J.; Leone, S. R. *J. Phys. Chem. C* **2011**, *115*, 6341−6349.
(17) Cordones, A. A.; Bixby, T. J.; Leone, S. R. *Nano Lett.* **2011**, *11*, 3366−3369.
(18) Kuno, M.; Fromm, D. P.; Hamann, H. F.; Gallagher, A.; Nesbitt, D. J. *J. Chem. Phys.* **2001**, *115*, 1028−1040.
(19) Chen, Y.; Vela, J.; Htoon, H.; Casson, J. L.; Werder, D. J.; Bussian, D. A.; Klimov, V. I.; Hollingsworth, J. A. *J. Am. Chem. Soc.* **2008**, *130*, 5026−5027.
(20) Tauc, J.; Grigorovici, R.; Vancu, A. *Phys. Status Solidi B* **1966**, *15*, 627−637.
(21) Mitzi, D. B.; Kosbar, L. L.; Murray, C. E.; Copel, M.; Afzali, A. *Nature* **2004**, *428*, 299−303.
(22) Dhingra, S. S.; Kanatzidis, M. G. *Inorg. Chem.* **1993**, *32*, 1350−1362.
(23) Mahler, B.; Spinicelli, P.; Buil, S.; Quelin, X.; Hermier, J.-P.; Dubertret, B. *Nat. Mater.* **2008**, *7*, 659−664.
(24) Dong, A.; Ye, X.; Chen, J.; Kang, Y.; Gordon, T.; Kikkawa, J. M.; Murray, C. B. *J. Am. Chem. Soc.* **2011**, *133*, 998−1006.
(25) Jasieniak, J.; Califano, M.; Watkins, S. E. *ACS Nano* **2011**, *5*, 5888−5902.
(26) Efros, A. L.; Rosen, M. *Annu. Rev. Mater. Sci.* **2000**, *30*, 475−521.
(27) Peng, X.; Schlamp, M. C.; Kadavanich, A. V.; Alivisatos, A. P. *J. Am. Chem. Soc.* **1997**, *119*, 7019−7029.
(28) Norris, D. J.; Bawendi, M. G. *Phys. Rev. B* **1996**, *53*, 16338−16346.
(29) Vela, J.; Htoon, H.; Chen, Y.; Park, Y.-S.; Ghosh, Y.; Goodwin, P. M.; Werner, J. H.; Wells, N. P.; Casson, J. L.; Hollingsworth, J. A. *J. Biophotonics* **2010**, *3*, 706−717.
(30) Ruimin, W.; Yanpeng, Z.; Chenli, G.; Muhammad, J.; Min, X. *Appl. Phys. Lett.* **2010**, *96*, 151107.
(31) Malko, A. V.; Park, Y. S.; Sampat, S.; Galland, C.; Vela, J.; Chen, Y. F.; Hollingsworth, J. A.; Klimov, V. I.; Htoon, H. *Nano Lett.* **2011**, *11*, 5213−5218.
(32) Zhao, J.; Nair, G.; Fisher, B. R.; Bawendi, M. G. *Phys. Rev. Lett.* **2010**, *104*, 157403.
(33) Galland, C.; Ghosh, Y.; Steinbruck, A.; Sykora, M.; Hollingsworth, J. A.; Klimov, V. I.; Htoon, H. *Nature* **2011**, *479*, 203−207.
(34) Htoon, H.; Malko, A. V.; Bussian, D.; Vela, J.; Chen, Y.; Hollingsworth, J. A.; Klimov, V. I. *Nano Lett.* **2010**, *10*, 2401−2407.
(35) Lifshitz, E.; Glozman, A.; Litvin, I. D.; Porteanu, H. *J. Phys. Chem. B* **2000**, *104*, 10449−10461.
(36) Chon, B.; Lim, S. J.; Kim, W.; Seo, J.; Kang, H.; Joo, T.; Hwang, J.; Shin, S. K. *Phys. Chem. Chem. Phys.* **2010**, *12*, 9312−9319.
(37) Horikoshi, S.; Abe, H.; Sumi, T.; Torigoe, K.; Sakai, H.; Serpone, N.; Abe, M. *Nanoscale* **2011**, *3*, 1697−1702.
(38) Nag, A.; Kovalenko, M. V.; Lee, J.-S.; Liu, W.; Spokoyny, B.; Talapin, D. V. *J. Am. Chem. Soc.* **2011**, *133*, 10612−10620.
(39) Li, J.; Chen, Z.; Wang, R.-J.; Proserpio, D. M. *Coord. Chem. Rev.* **1999**, *192*, 707−735.
(40) Peterson, J. J.; Nesbitt, D. J. *Nano Lett.* **2009**, *9*, 338−345.
(41) Spinicelli, P.; Buil, S.; Quelin, X.; Mahler, B.; Dubertret, B.; Hermier, J. P. *Phys. Rev. Lett.* **2009**, *102*, 136801.
(42) Konstantatos, G.; Sargent, E. H. *Nat. Nanotechnol.* **2010**, *5*, 391−400.